ACS OMEGA

http://pubs.acs.org/journal/acsodf

Article

Evaluating Use of Boron- and Hafnium-Modified Polysilazanes for Ceramic Matrix Minicomposites

Shakir Bin Mujib,* Mohammed Rasheed, and Gurpreet Singh

Cite This: *ACS Omega* 2022, 7, 45325−45335

Read Online

ACCESS | Metrics & More | Article Recommendations | Supporting Information

ABSTRACT: In this study, the potential of polymer-derived ceramic matrix composites (CMCs) is demonstrated by the addition of thin ceramic coatings on carbon fiber (CF) bundles. Boron- and hafnium-modified polysilazane liquid precursors were synthesized and used to infiltrate the fiber bundles of CF to fabricate lab-scale Si(B)CN/CF and Si(Hf)CN/CF CMC minicomposites, respectively by crosslinking and then pyrolysis at 800 °C. The crosslinked precursor to ceramic yield was observed to be as high as 90% when the procedure was carried out in inert environment. The Si(B)CN/CF contained Si−N and B−N bonds, while Si−N and Hf−O−Si bonds were observed for the Si(Hf)CN/CF sample with uniform and dense surfaces. Room-temperature tensile tests showed that the Si(Hf)CN/CF sample could reach a tensile strength of ∼790 MPa and an elastic modulus of 66.88 GPa among the composites. An oxidation study of the Si(Hf)CN/CF minicomposites showed higher stability compared to SiCN/CF and Si(B)CN/CF minicomposites up to 1500 °C.

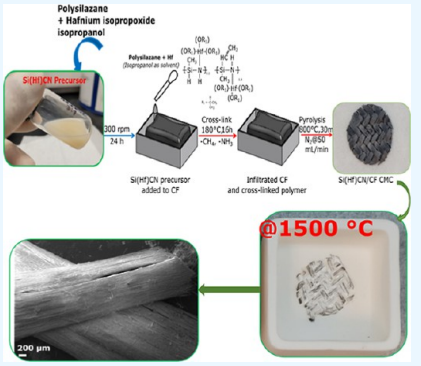

1. INTRODUCTION

CMCs are suitable candidates for extreme environment applications due to their low density, high limit of damage tolerance, and higher use temperature capability.[1] Turbine engine blades and rocket nozzles require new materials to increase operational temperatures while maintaining a lightweight structure. CMCs are capable of satisfying the high-temperature requirements in a lightweight structural form.[2] The requirement for high-temperature materials with considerable mechanical strength for jet engines was recognized early; however, the necessary step was to manufacture CMCs which would be suitable for their modest high-temperature strength and oxidation resistance, such as C/C−ZrC composites,[3] C/C−SiC composites,[4] or metal−ceramic interpenetrating phase composites,[5] and so forth.

Ceramic monoliths and conventional ceramics such as SiC or Si_3N_4, manufactured via powder processing technology, have shown exceptional oxidation resistance above 1000 °C in a low-density form.[6] However, the brittle nature of these ceramics prevents machining. On the other hand, Si-based polymeric precursors, commonly known as poly(organosilazanes), poly(carbosilane), and poly(organosiloxane), transform into complex ceramic materials such as SiCN, SiC, and SiOC upon controlled thermal decomposition.[7] These covalently bonded molecular precursor-derived ceramics (PDCs) differ from traditional ceramics. PDCs have processing flexibility that allows them to achieve any desired shape, control of nanostructure of the final ceramic product (by tuning the precursor chemistry), low processing temperature, and the ease of composite fabrication.[8] In addition, elemental doping and the addition of fillers, including B,[9] Al,[10] ZrO_2,[11] TiO_2,[12] and HfO_2,[13] are possible for PDCs. Depending on the elemental configurations, Si-based PDCs can be used in various high-temperature applications involving coatings, sensors, reinforcement, or matrices.[14] On the other hand, carbon fiber (CF) reinforcement is used in CMCs to prevent matrix crack propagation and improve thermal shock and impact resistance.[15] CFs are capable of retaining their mechanical properties at low-to-moderate temperatures[16] and have a low cost compared to fine ceramic fibers. Recent studies have shown that due to their relatively low cost along with high thermal and electrical conductivity, and large specific surface area, CFs/carbon materials have also found use in batteries,[17] sensors,[18] optoelectronics,[19] solar cells,[20] etc.

Quaternary PDCs of Si(X)CN (where X = B, Hf, or Al) are of particular interest due to their exceptional structural and chemical stability at elevated temperatures. Such PDCs remain X-ray amorphous up to 1500 °C, show excellent creep resistance, and are stable up to approximately 2000 °C.[8,21] These unique properties have been attributed to the presence of persistent nanodomains (generally ranging from ∼10−20 Å) and aromatic carbon in their structure that tends to resist crystallization. The molecular structure of the polymer precursor also directly influences the properties of pyrolyzed

Received: September 12, 2022
Accepted: November 24, 2022
Published: December 5, 2022

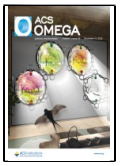

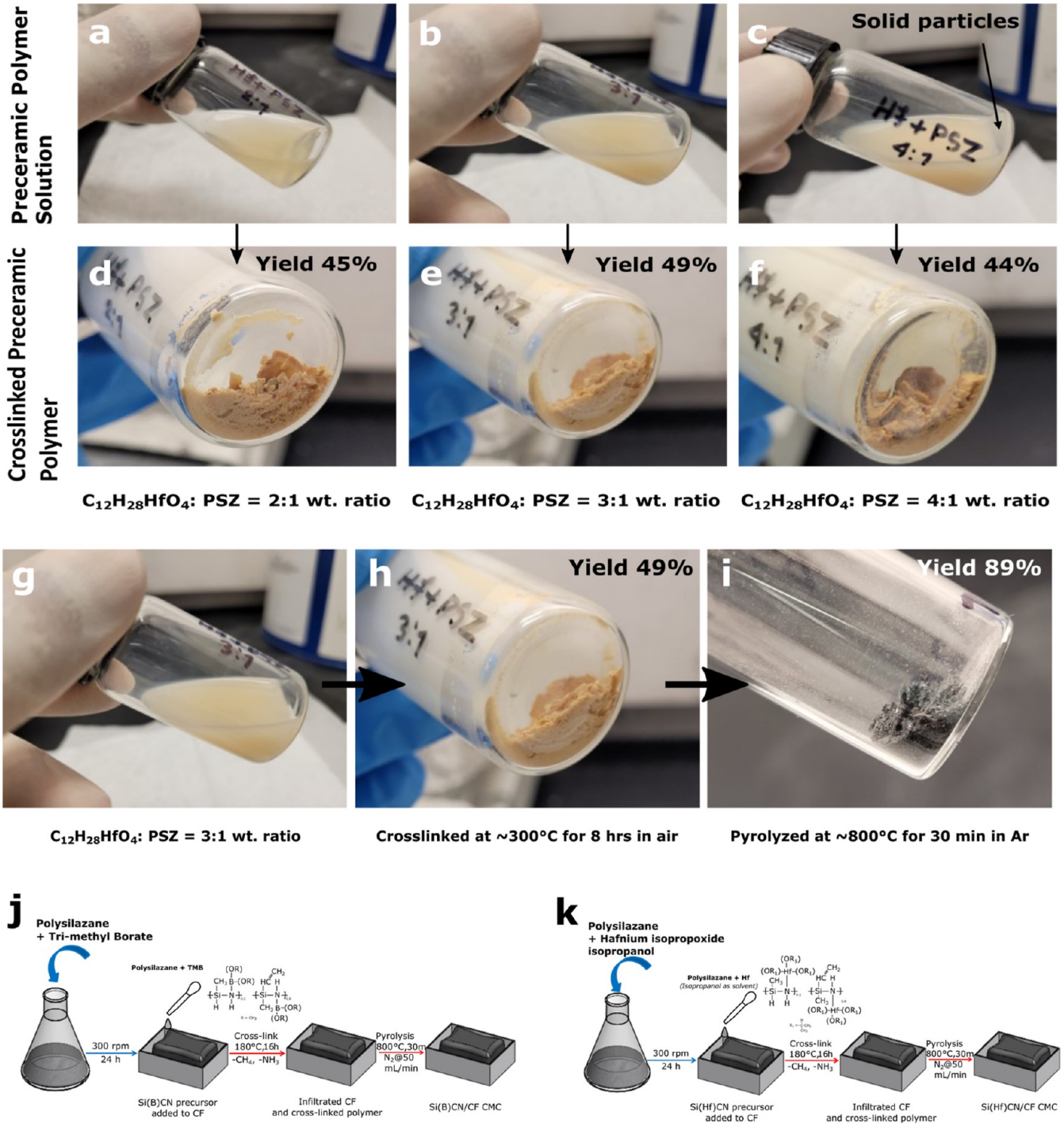

Figure 1. Digital camera images: (a−c) solubility of hafnium isopropoxide isopropanol in PSZ with different concentrations (top) and (d−f) their corresponding crosslinked powders (bottom). Yield represents preceramic precursor solution to crosslinked polymer conversion (by mass). Camera images of the optimized Hf-modified PSZ from (g) preceramic polymer precursor to (h) crosslinked and (i) ceramic Si(Hf)CN powder. Yield represents the polymer-to-ceramic conversion (by mass). Schematics show coating, crosslinking, and pyrolysis process of PDC/CF CMCs: (j) synthesis process of Si(B)CN/CF and (k) Si(Hf)CN/CF ceramic minicomposites.

ceramic. Controlling the amount of free carbon phase and size of the various nanodomains (e.g., Si_3N_4, SiC, and h-BN) in these ceramics could help tailor their high-temperature, chemical, thermal, and mechanical properties. Such nanodomain microstructure is not possible via chemical vapor deposition or related techniques.[22]

Typically, boron-containing PDCs have much higher chemical and thermo-mechanical stability than boron-free counterparts. Although the molecular structure of Si(B)CN is not fully understood, the h-BN phase may increase the free activation energy for crystallization and Si−N reaction with C. Given that PDCs can be conveniently prepared by controlled heating and chemical modifications of liquid-phase polymers to take any desired shape, they are useful for defense and aerospace applications.[8,23,24] Lee et al. incorporated polymer infiltration and pyrolysis (PIP) to synthesize Si(B)CN CMCs

https://doi.org/10.1021/acsomega.2c05916
ACS Omega 2022, 7, 45325−45335

that were stable up to 1500 °C in an Ar atmosphere.[25] Weinmann et al. used Si(B)CN ceramics from a boron-modified polysilazane (PSZ) precursor to show that the ceramic was stable up to 2000 °C in thermogravimetric analysis (TGA) in an inert gas atmosphere.[26] According to the authors, substantial amounts of Si_3N_4 can affect the high-temperature stability due to the decomposition of Si(B)CN into N_2 and SiC. Kong et al. showed that Si(B)CN ceramics could retain the amorphous structure up to 1600 °C with a boron atomic composition of 6−8.5% in the final ceramic structure.[27] Zhao et al. used sodium borohydride as a boron source to achieve Si(B)CN ceramic, which showed a dense and smooth surface after annealing at 1400 °C.[28] In this liquid-precursor approach, the poly(boro)silazane containing active group Si−H was synthesized via reactions with dichloromethylvinylsilane, hexamethyldisilazane, sodium borohydride, and dimethyl chloro vinyl silane under the inert atmosphere.

Similar to Si(B)CN, ceramic composites based on Si(Hf)CN show promising resistance at high-oxidation temperatures. Ionescu et al. reported improved thermal stability for SiOC/HfO_2 ceramic above 1000 °C compared to hafnia-free SiOC.[29] Thermal stability of the SiOC/HfO_2 nanocomposites was contributed to the in situ formation of $HfSiO_4$ at elevated temperatures. Sun et al. also presented a similar phenomenon in a SiOC-/HfO_2-based ceramic composite derived from polymethylsiloxane modified by various HfO_2 polymorphs.[13] Wen et al. reported the laser ablation behavior of SiHfC-based ceramics prepared from a single-source precursor.[30] They showed that the incorporation of Hf into the SiC-based ceramics enables the composites to withstand ultrahigh temperature (approx. 3000 °C) in a short period of time (0.5 s) proving the excellent thermal shock resistance of the SiHfC-based ceramics.

Previous works on this topic have primarily focused on use of liquid precursors from multiple sources to fabricate bulk quaternary ceramics[25,26,28,31] and/or employed elaborate techniques such as PIP, mechanical alloying and hot-press sintering, and spark plasma sintering to fabricate CMCs.[28,30,32,33] This study intended to bridge the gap between the processibility of precursors for quaternary ceramics and their use in fabricating advanced CMCs. The current work aimed to study the efficacy of the infiltration process of CF cloth or minibundles of CFs by single-source liquid-phase precursors of Si(B)CN and Si(Hf)CN and the effect on the morphology, mechanical property, and oxidation stability of the minicomposites. Here, a PSZ-based precursor was mixed with boron- and hafnium-containing precursors to synthesize Si(B)CN and Si(Hf)CN polymeric precursors, respectively. The homogeneous solutions of the precursors were then allowed to infiltrate CF cloth via a drop-coating process mimicking a lab-scale polymer infiltration process and then crosslinked and pyrolyzed to achieve Si(B)CN/CF and Si(Hf)CN/CF ceramic minicomposites. For comparison purposes, SiCN/CF minicomposites were also fabricated using the PSZ precursor. Several characterization techniques, such as scanning electron microscopy (SEM), Raman and Fourier transform infrared (FTIR) spectroscopy, and X-ray photoelectron spectroscopy (XPS), were used to evaluate the polymer-to-ceramic evolution and microstructures in SiCN/CF, Si(B)C/CF, and Si(Hf)CN/CF ceramic composites. Preliminary mechanical tests performed on the composite bundle showed that Si(Hf)CN/CF had the highest tensile strength of 790 MPa and elastic modulus of 66.88 GPa among the ceramic minicomposites. An oxidation study in ambient air of the ceramic minicomposites showed sample stability up to 1500 °C. Structural and compositional changes of the oxidized samples were investigated via XPS and SEM analyses.

2. EXPERIMENTAL SECTION

2.1. Materials. A commercially available CF cloth was used in this study as the reinforcement phase [6K, 2 × 2 Twill Weave CF (Fibre Glast Developments Corporation, USA)]. According to the manufacturer, the fiber has a thickness of 0.017 in. and a weight of 10.9 oz/sq yd.

The PSZ ceramic precursor, Ceraset PSZ 20 (PUMVS/Ceraset), was obtained from Clariant Corporation, USA. Trimethyl borate (TMB) (≥98%, MW 103.91 g mol^{-1}) and hafnium isopropoxide isopropanol ($C_{12}H_{28}HfO_4$) (99.9%, MW 414.84 g mol^{-1}) were purchased from Sigma-Aldrich, USA. For the preparation of coating solutions, isopropanol (≥99.9%, MW 60.096 g mol^{-1}) from Fisher Scientific, USA, was used as the solvent.

2.2. Preparation and Optimization of Preceramic Polymer Precursor for Si(B)CN and Si(Hf)CN Ceramics. *2.2.1. Si(B)CN−Preceramic Polymer.* Boron-modified silazane was prepared following procedures described in a patent by authors.[23] Boron reagent TMB was added in a drop-wise manner to poly(ureamethylvinyl)silazane (commercial name: Ceraset) in a large beaker at a slow rate of ∼1 mL/min, while poly(ureamethylvinyl)silazane was stirred at 300 rpm overnight. The overall concentration of boron reagent to Ceraset was approximately 1:1 wt %. The preceramic polymer's rheology sufficiently allowed wetting of the CFs.

2.2.2. Si(Hf)CN−Preceramic Polymer. Hf-modified silazane was prepared following a similar procedure as described in the previous section. Since the rheology, polymer-to-ceramic yield, and the optimum loading of Hf in PSZ were not known, a study involving three different mass ratios of Hf reagent to PSZ was conducted (Figure 1a−f). As shown in the results in Figure 1b, the 3:1 mass loading of Hf reagent in PSZ led to the preceramic polymer reaching a saturation limit. Any further additions of Hf reagent led to precipitation in the PSZ (Figure 1c). The precursor-to-ceramic stages of the 3:1 mass loading are shown in Figure 1g−i.

2.3. Preparation of PDC/CF Ceramic Minicomposites. Circles with an approximate diameter of 19 mm were cut from the CF cloth (∼100 mg) with a metal punch. The preceramic polymer solutions (PSZ, B-modified silazane for Si(B)CN ceramic, and Hf-modified silazane for Si(Hf)CN ceramic) were then injected using pipettes (approx. 1 mL) to infiltrate the CF circular discs entirely. Consequently, approximately 0.25 mL of preceramic polymer was used for approximately 25 mg of CFs. The infiltration procedure of the CF samples was performed in an Ar-filled glovebox to avoid premature oxidization of the samples. The samples were then cross-linked in air (300 °C, 8 h in an oven) or Ar (180 °C, 16 h in a glovebox). Finally, the samples were pyrolyzed in a N_2 atmosphere at 800 °C for 30 min, resulting in PDC/CF ceramic minicomposites (cited as CMCs), as shown in Figure 1j,k.

The as-fabricated PDC/CF CMCs are shown in Figure 2a−c. The preceramic polymer-coated fibers were crosslinked in two different environments (in air at 300 °C and in an Ar environment at 180 °C) to achieve ideal ceramic coatings and yield on the CFs. Crosslinking (XL) in Ar provided the best result in terms of ceramic yield from the polymeric precursor. As a result, further experiments were conducted only on

https://doi.org/10.1021/acsomega.2c05916
ACS Omega 2022, 7, 45325−45335

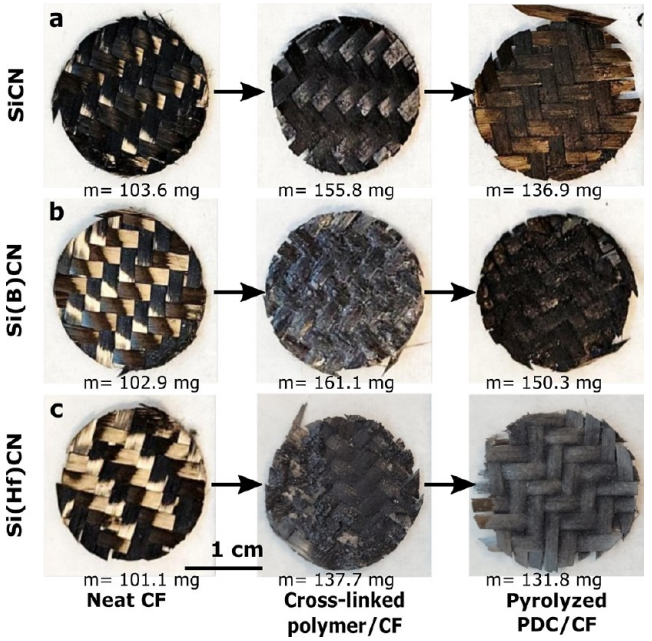

Figure 2. Digital camera images of CFs coated with (a) PSZ, (b) boron-modified PSZ, and (c) hafnium-modified PSZ before coating, after crosslinking, and after pyrolysis. Crosslinking is done at 180 °C in an Ar environment, and pyrolysis is done at 800 °C in a N_2 environment.

samples fabricated in an inert environment. Polymer-to-ceramic conversion yield (by weight) of various CMC samples is presented in Table 1.

Table 1. Conversion Yield of Coated Samples by Weight from the Crosslinked Polymer-to-Ceramic Stage

sample	wt yield (%)
SiCN/CF (XL in air)	88
Si(B)CN/CF (XL in air)	72
Si(Hf)CN/CF (XL in air)	41
SiCN/CF (XL in Ar)	89
Si(B)CN/CF (XL in Ar)	94
Si(Hf)CN/CF (XL in Ar)	98

2.4. Characterization Techniques. This study utilized several characterization techniques to determine the morphology, composition, and chemical compositions of the samples at various stages of fabrication of the CMC minicomposites. The surface morphology of the samples was studied using SEM on a Carl Zeiss EVO MA10 system with an incident voltage of 5 kV.

The surface composition was analyzed by XPS using a Thermo Scientific Al Kα X-ray source (beam energy = 1486.6 eV and spot size = 400 μm). An initial sputtering with Ar^+ at 3.0 keV (current ~ 4 μA cm^{-2}) for 2 min was performed on the surface of the ceramic-coated fibers to remove the surface contamination. Under these conditions, the materials removed was approx. 1.6 nm.

Molecular structure and chemical evolutions of the CMCs were determined via Raman spectroscopy and FTIR. A confocal micro-Raman microscope (HORIBA Jobin Yvon LabRam ARAMIS) equipped with a HeNe laser source (632.8 nm) was used to conduct Raman analysis in the range of 800−2000 cm^{-1} to determine the carbon vibrational modes. The presence and evolution of various chemical functional groups of the silazane precursors in the composites were investigated using a Perkin Elmer Spectrum 400 FTIR spectrometer in the range of 500−2500 cm^{-1}.

To determine the mechanical properties of composites, tensile tests of the CMCs were performed using a Shimadzu AGS-X Universal Testing Machine with a 5 kN load cell. To understand the oxidation stability of the CMCs, the samples were heated to 800, 1000, 1200, and 1500 °C in stagnant air in a SentroTech box furnace with a heating rate of 5 °C min^{-1}.

3. RESULTS AND DISCUSSION

SEM micrographs of the CMC minicomposites revealed the surface features and coating thickness of the samples. SEM images of SiCN/CF, Si(B)CN/CF, and Si(Hf)CN/CF ceramic composite samples are shown in Figure 3. Figure 3a compares the uncoated CFs and individual fiber specimen before the ceramic coating; the CMC samples showed shiny, uniform, and continuous ceramic coatings on the surfaces. As shown in Figure 3b, the SiCN-coated fibers after pyrolysis were clearly discernible from the uncoated fibers before pyrolysis. The Si(B)CN coating had a smooth, continuous surface free

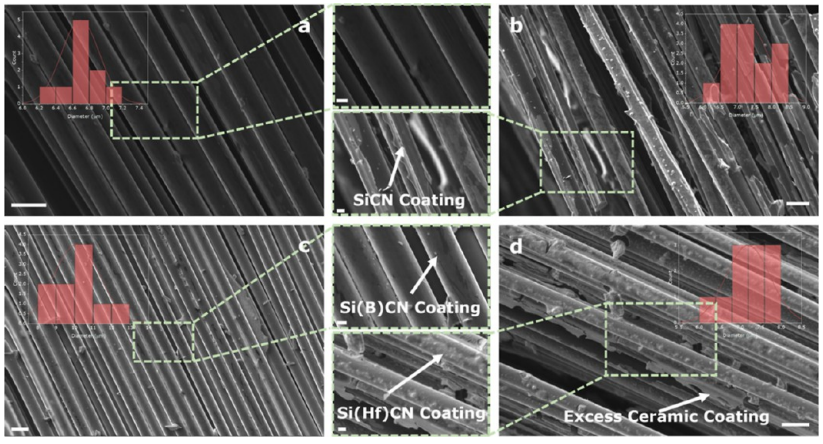

Figure 3. SEM images of CFs with individual fibers before and after ceramic coatings; (a) uncoated CFs, (b) continuous SiCN coating on the CFs, (c) comparatively thicker ceramic coating (2−4 μm) of Si(B)CN/CF, and (d) protruding ceramic coatings for Si(Hf)CN/CF indicating an excess amount of preceramic polymers are infused during the coating process. The scale bar is 10 μm (inset scale bar is 2 μm).

https://doi.org/10.1021/acsomega.2c05916
ACS Omega 2022, 7, 45325−45335

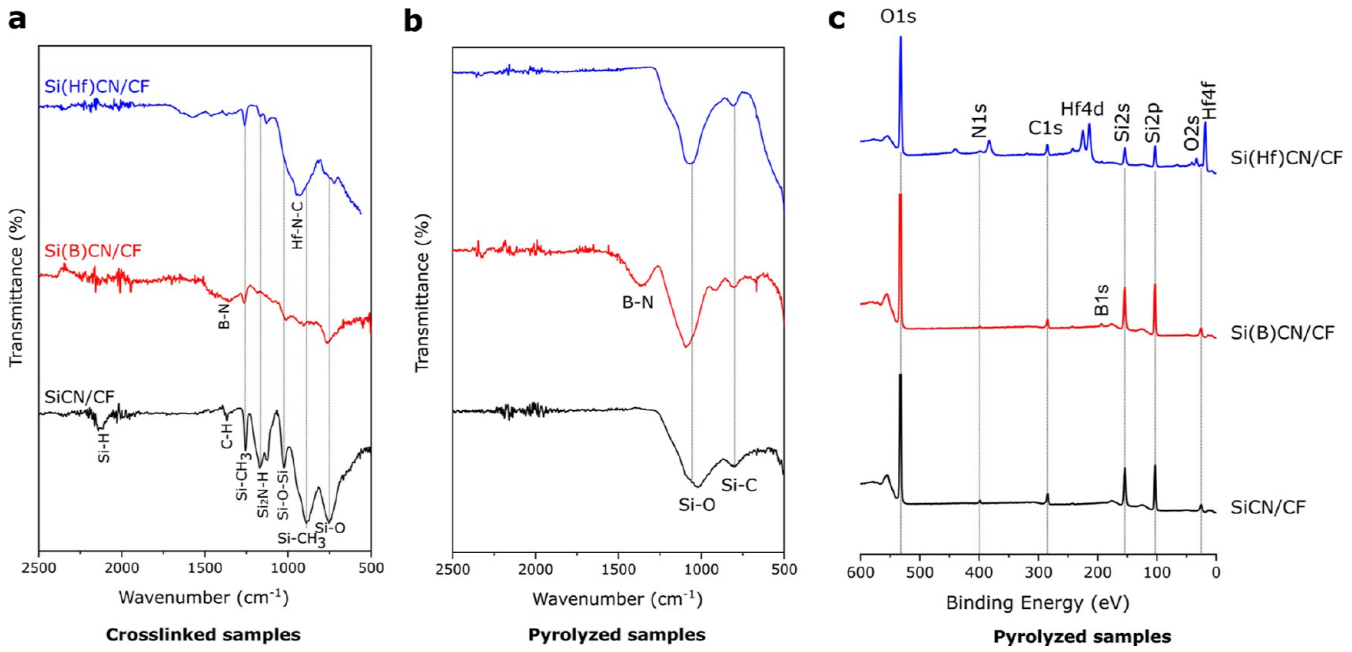

Figure 4. FTIR spectra of ceramic composites after (a) crosslinking and (b) pyrolysis show the evolution of chemical bonds in the ceramic coatings from the polymer to pyrolyzed stages and (c) XPS survey spectra of CMC samples. Presence of Si, B, Hf, and N confirms the Si(B)CN and Si(Hf)CN ceramic coating on the fibers. XPS of SiCN-/CF-coated fibers is included for comparison purposes.

from defects, as shown in Figure 3c. However, for Si(Hf)CN-coated fibers (Figure 3d), ceramic coatings were observed to stick out of the fiber surface coatings after pyrolysis, which is the result of an excessive deposit of preceramic polymers into the CF disc during the coating process. For uncoated CFs, the average fiber diameter was measured to be 6−7 μm. For SiCN/CF, Si(B)CN/CF, and Si(Hf)CN/CF CMCs, the average diameter was 7−8, 9−12, and 7−8 μm, respectively.

Raman spectra of the CMC samples showed the presence of carbon domains to evaluate the corresponding microstructures in the composite materials. As shown in Figure S3, the D and G vibrational bands at 1342 and ∼1600 cm^{-1}, respectively, suggested the presence of free carbon structures. The D peaks indicated disordered bands that originated in structural defects and aromatic rings, whereas G peaks were associated with in-plane stretching of sp^2-hybridized carbon atoms.[34] However, the D and G peaks were not pronounced in the Si(Hf)CN/CF sample. This phenomenon was attributed to the strong fluorescence background that was produced under the visible laser source (HeNe 632.8 nm). XPS analysis was later performed to confirm the presence of carbon domains in the Si(Hf)CN/CF sample.

FTIR spectra in Figure 4a,b show the characteristic absorption bands of the polymer-to-ceramic conversions of the SiCN/CF, Si(B)CN/CF, and Si(Hf)CN/CF samples. For the crosslinked samples in Figure 4a, the peaks at ∼1060 and ∼1260 cm^{-1} corresponded to the stretching of Si−O−Si and Si−CH_3, respectively, in the CMCs.[35] These peaks indicated the presence of Si precursors in the composite samples. For Si(B)CN/CF and Si(Hf)CN/CF samples, the decreased Si−CH_3 and Si_2N−H (∼1175 cm^{-1}) peak intensities were contributed to the increased crosslinking of the samples at 180 °C. A broad peak of the B−N functional group formed in the Si(B)CN/CF sample and became more intense after pyrolysis (Figure 4b).[36] A characteristic absorption band of Hf−N−C (∼945 cm^{-1}) was found in the crosslinked Si(Hf)CN/CF sample, which was overlapped with the Si−CH_3 peaks.[6] After pyrolysis, the CMC samples showed two main peaks of Si−O (∼1060 cm^{-1}) and Si−C (∼800 cm^{-1}), as presented in Figure 4b. The presence of these two obvious peaks in all the samples confirmed the existence of ceramic coatings in the composites.[37] All characteristic bands of the H-containing functional groups also disappeared, indicating the conversion of polymer coatings to ceramic materials.

XPS was performed to determine the elemental composition of the CMC samples and to characterize bonding of the molecules present in the samples. As presented in Figure 4c, XPS survey scan showed Si 2p, C 1s, and O 1s peaks in all the samples, thereby confirming the presence of ceramic coating on the CFs. An additional B 1s peak was found for the Si(B)CN/CF samples, but the N 1s peak intensity was suppressed in the survey scan of Si(B)CN/CF. For the Si(Hf)CN/CF sample, the Hf peaks confirmed the presence of Si(Hf)CN coating on the CFs. Surface compositions of the CMC samples were determined by integrating the area under the respective elemental peaks and are presented in Table 2.

Table 2. Elemental Composition of the CMC Samples Determined by XPS

	elements (at. %)					
pyrolyzed samples	Si	C	N	O	B	Hf
SiCN/CF	41.33	9.84	1.32	47.51	NA	NA
Si(B)CN/CF	40.34	6.84	0.55	49.00	3.27	NA
Si(Hf)CN/CF	28.63	13.56	1.51	48.12	NA	8.18

Figure 5 shows the bonding of various elements in the CMC samples. Fitted peaks under the Si 2p (Figure 5a,e,j) for all the samples primarily showed the presence of Si−N (102.1 eV)[28] and Si−C (100.6 eV)[28,38] bonds, which confirmed the uniform distribution of ceramic coatings on the surface of the CFs. A minimal amount of Si was bonded to oxygen. Low intensity of

https://doi.org/10.1021/acsomega.2c05916
ACS Omega 2022, 7, 45325−45335

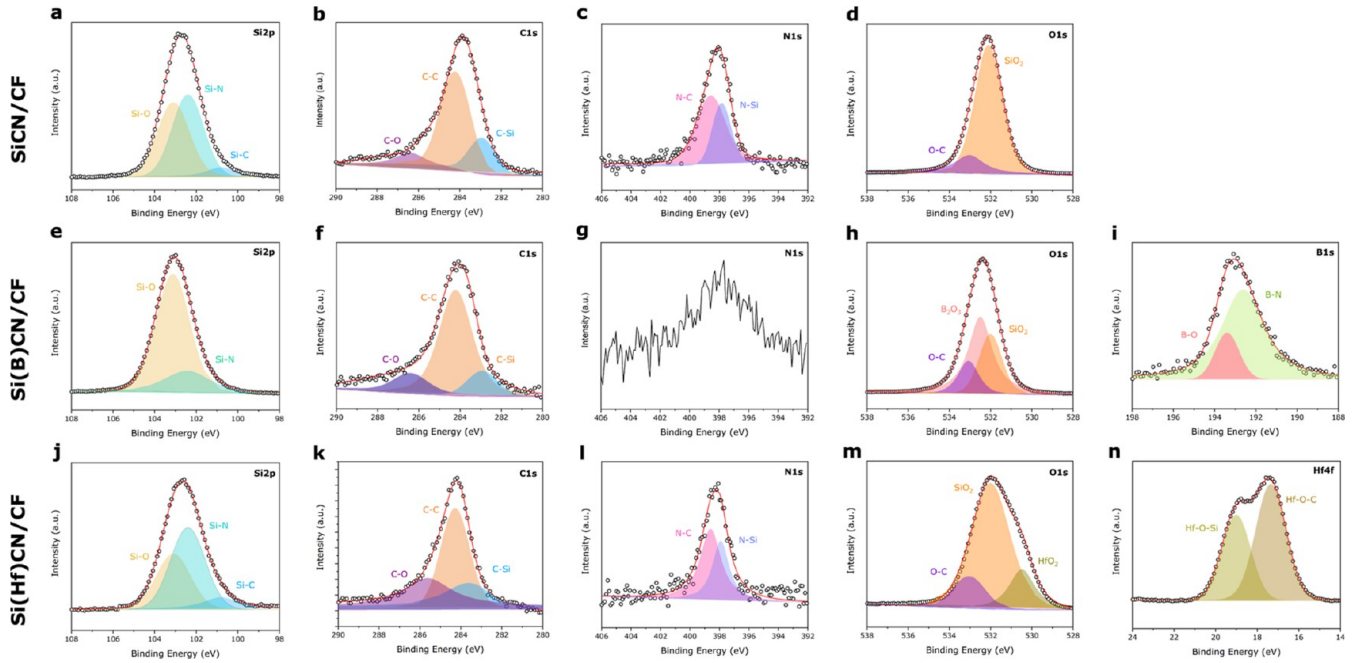

Figure 5. High-resolution XPS spectra of the CMC samples for Si 2p, C 1s, N 1s, O 1s, B 1s, and Hf 4f and (a–d) SiCN/CF, (e–i) Si(B)CN/CF, and (j–n) Si(Hf)CN/CF.

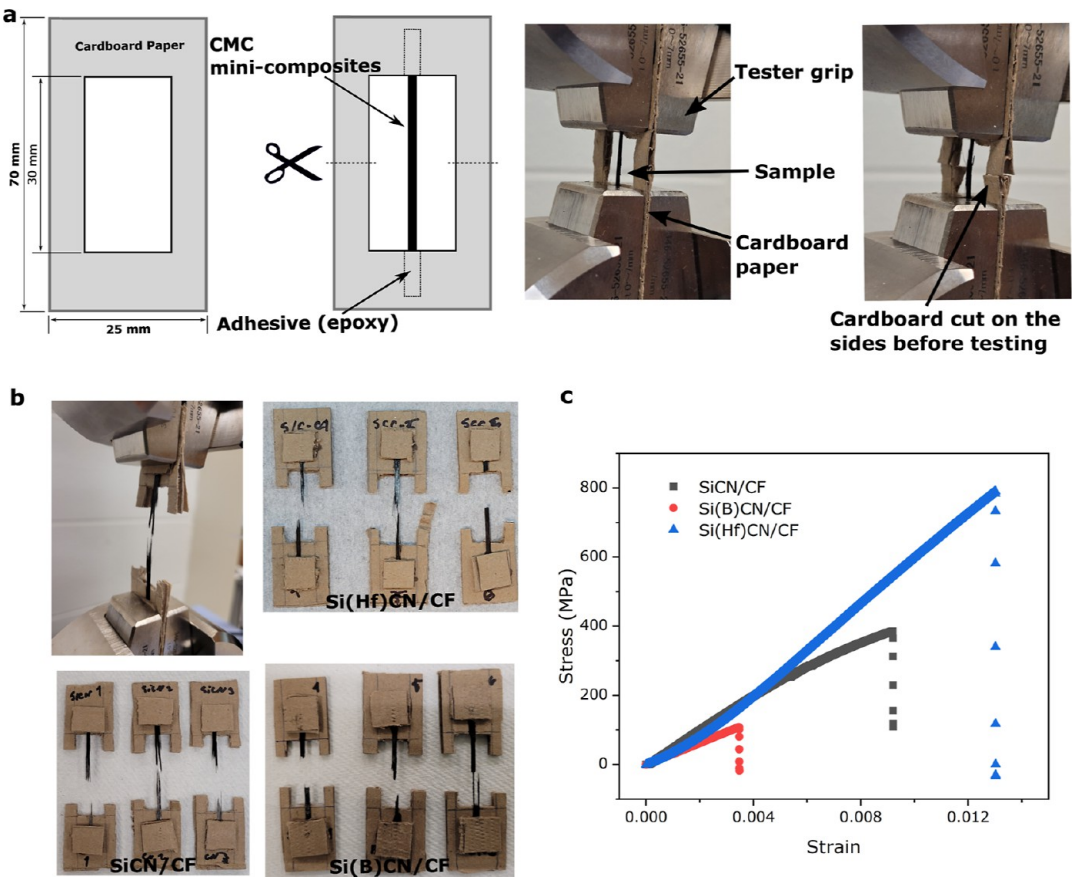

Figure 6. Tensile test of the PDC/CF composites: (a) schematic and digital image of the tensile test setup. Samples are mounted on cardboards which are cut prior to the tests. (b) Example of a tested sample. One batch of samples tested for SiCN/CF, Si(B)CN/CF, and Si(Hf)CN/CF minicomposites is shown counter-clockwise. (c) Stress vs strain plots of the CMC samples. The tensile strength of the uncoated CF bundles was also measured for comparison purposes and is presented in Figure S4.

the C–Si (282.9 eV)[39] bond under the C 1s peak in SiCN/CF (Figure 5b) and Si(B)CN/CF (Figure 5f) was attributed to the low carbon content of the samples. In addition, C–C (284.2 eV)[28] and C–O (286.4 eV)[28,38] were observed in the C

https://doi.org/10.1021/acsomega.2c05916
ACS Omega 2022, 7, 45325–45335

1s band.[40] The intense peaks for C−C suggested that most of the carbon phase in the ceramic coating was free carbon. As shown in Figure 5g, the N 1s peak in the Si(B)CN/CF sample was not fitted due to the low nitrogen content in the sample, as indicated by the survey XPS. In the O 1s bands (Figure 5d,h,m), additional peaks for B_2O_3 (532.5 eV)[41] and HfO_2 (530.4 eV)[42] were observed for the Si(B)CN/CF and Si(Hf)CN/CF samples, respectively. In the Si(B)CN/CF sample, boron (Figure 5i) was primarily bonded to nitrogen (B−N) and oxygen (B−O).[43] The Hf 4f band (Figure 5n) was fitted with two intense peaks at 19.6 and 17.8 eV that corresponded to Hf−O−Si and Hf−O−C, respectively.[44]

3.1. Mechanical Properties. Mechanical properties of the CMC minicomposites were determined by the tensile test of the composite bundles. Rectangular composite bundle samples were prepared using CF bundles collected from the CF cloth. Each bundle contained 6000 individual CFs. The composites were mounted onto cardboard tabs using epoxy for the tests as reported in previous works.[45] Each cardboard tab had a 30 mm slot in the middle, which was the gauge length of the tensile specimens, as shown in Figure 6a. The cardboard tabs were cut on the sides after mounting the samples in the tester and prior to load application. During tests, the load was applied at a rate of 0.2 mm/min to maintain a quasi-static tensile condition.

The tensile behavior of the samples is shown in Figure 6c, and the results are reported in Table S1. The Si(Hf)CN/CF composite showed the highest average strength of 790 MPa, followed by SiCN/CF and Si(B)CN/CF samples with average strengths of 390 and 110 MPa, respectively. The Si(Hf)CN/CF sample also showed the highest Young's modulus of 66.88 GPa, whereas the SiCN/CF and Si(B)CN/CF composites showed Young's moduli of 49.89 and 30.58 GPa, respectively. These values are higher than that of the SiC/CF CMCs reported in the literature.[46] The tensile strength of the uncoated CF bundles was also measured for comparison purposes and is presented in Figure S4. The average tensile strength of the uncoated fibers was measured to be 2.3 GPa, which was higher than that of the composites. This behavior is typical in PIP-processed composites where the strength of the composite is lower than that of the pristine fibers.[47] Typically, there is a higher amount of porosity and cracks in the composites with a single layer of ceramic coating. As a result, the tensile strength is lower for the minicomposites. This low strength behavior is also primarily due to localized stress concentration on adjacent fibers (induced from the cracks in the matrix of a CMC).

Crack formation in CMC matrix typically occurs during the hydrogen evolution and transformation into the ceramic phase. In addition, mechanical and thermal damage of the fibers during composite processing results in low strength of the composite.[48] The average tensile strength of the heated CFs (at 800 °C in a N_2 environment) was 0.45 GPa (presented in Table S1), which was almost 5 times lower than the strength of neat uncoated CFs. The strain-to-failure of the composites was also lower than the uncoated fibers, indicating the abrupt mechanism of fracture of the samples. This fracture behavior was also confirmed by post-tensile SEM of the samples, as shown in Figure S5.

3.2. Oxidation Stability. The oxidation behaviors of PDC/CF minicomposites at various oxidation temperatures are shown in Figure 7. The samples were oxidized at 800, 1000, 1200, and 1500 °C in stagnant air, which were labeled PDC/CF800, PDC/CF1000, PDC/CF1200, and PDC/CF1500, respectively. The uncoated CFs were used as a contrast sample with the ceramic composites in an oxidation experiment. Results showed that the PDC/CF samples survived the high oxidation environments, whereas the uncoated CFs did not. Figure 8 also shows that the SiCN/CF samples started disintegrating above 1000 °C, whereas the Si(B)CN/CF samples exhibited deformation in the shape. The Si(Hf)CN/CF sample turned white on the surface, indicating the formation of HfO_2.[49] The weight retention of the samples after oxidation is reported in Table 3. The Si(B)CN/CF samples showed highest resistance to oxidation in terms of weight retention, while the Si(Hf)CN/CF samples showed less retention with more uniform weight changes and less-significant differences at higher temperature.

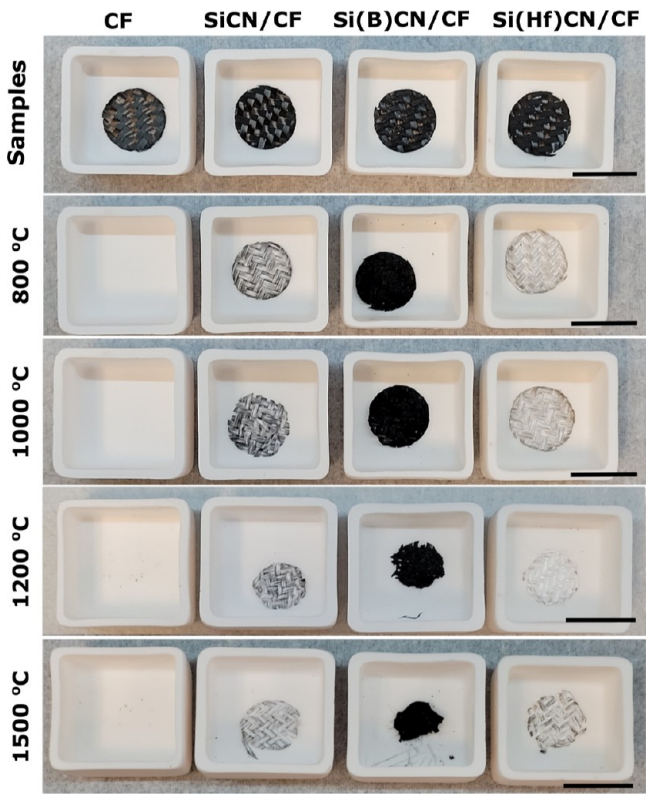

Figure 7. Postoxidation behavior of the uncoated CF and PDC/CF samples at various temperatures. The PDC/CF samples show high resistance to oxidation up to 1500 °C. Scale bar is 2 cm.

Morphology of the oxidized CMCs was obtained, as shown in Figure 8. The SEM of each composite was evaluated to delineate the oxidation behavior of the CMCs after heating. For SiCN/CF samples, the composites began disintegrating and the fibers dispersed after heating at 1000 °C, as shown in the SEM micrographs of SiCN/CF1200 and SiCN/CF1500 samples in Figure 8. These results correspond to the oxidized sample digital images in Figure 7. For Si(B)CN/CF samples, the composites showed shape deformation and shrinkage after 1200 °C. The SEM image of the Si(B)CN/CF1500 sample indicated that the composite structure melted at 1500 °C and formed a thin film. However, Si(Hf)CN/CF samples showed high oxidation resistance up to 1500 °C, and the fiber−matrix structures of the samples showed minimal damage, even at 1500 °C. TGA was performed using NETZSCH TG 209F1 Libra in an open crucible; the sample was heated to 1000 °C at a rate of 10 °C/min. Based on the final mass retention of 69%

https://doi.org/10.1021/acsomega.2c05916
ACS Omega 2022, 7, 45325−45335

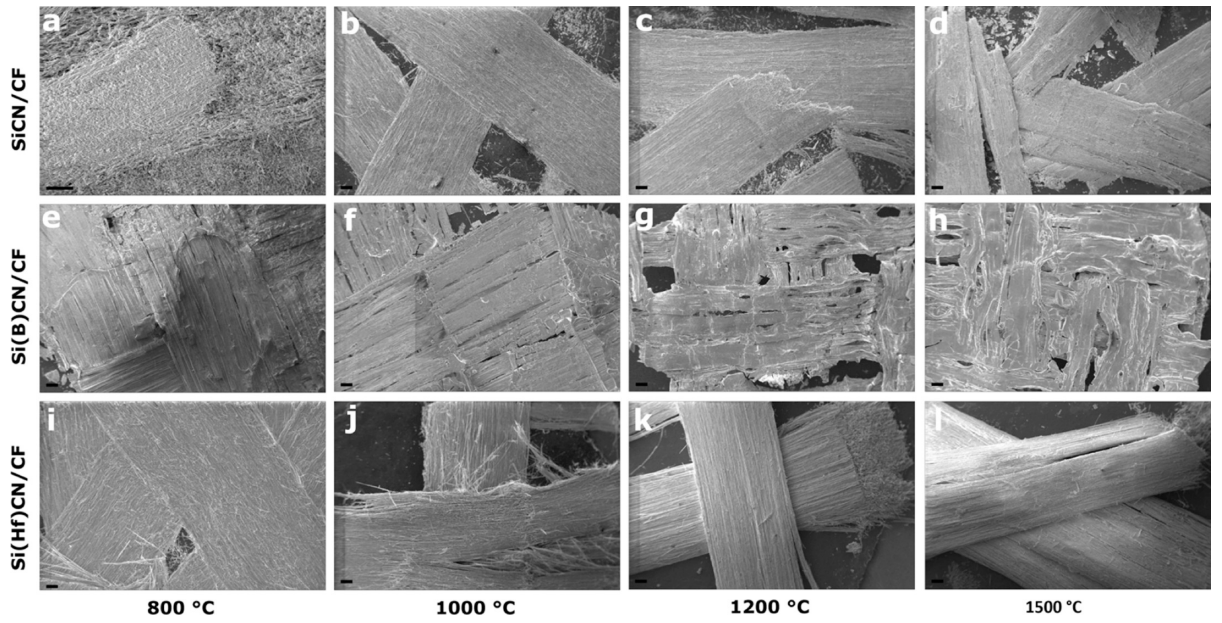

Figure 8. SEM micrograph of the oxidized PDC/CF samples at various temperatures. (a,b,c,d) SiCN/CF samples oxidized at 800, 1000, 1200, and 1500 °C, respectively; (e,f,g,h) Si(B)CN/CF samples oxidized at 800, 1000, 1200, and 1500 °C, respectively; and (i,j,k,l) Si(Hf)CN/CF samples oxidized at 800, 1000, 1200, and 1500 °C, respectively. Scale bar is 200 μm.

Table 3. Weight Retention of PDC/CF Samples after Oxidation at Various temperatures

	weight retention (%)			
sample	800 °C	1000 °C	1200 °C	1500 °C
SiCN/CF	20	20	18	18
Si(B)CN/CF	35	34	33	30
Si(Hf)CN/CF	27	21	20	19

for CMC and 4% for the neat CF (Figure S6), it is assumed that approx. 35% of the CFs in PDC/CF CMC was not protected by the ceramics against oxidation.

To validate these results, the oxidation behavior of PDC/CF composites at various oxidation temperatures was also evaluated by XPS. Table 4 presents the elemental composition of the oxidized samples at different temperatures. The increased amount of oxygen in all the samples indicated the oxidation levels of the CMC samples. The most significant increase occurred for the SiCN/CF samples due to the oxidation of SiC and Si_3N_4 in the composites, leading to the formation of SiO_2 and eventually decreased stability.[50]

Oxidation of the Si(B)CN/CF samples resulted in the formation of SiO_2 and B_2O_3.[51] The borosilicate (B_2O_3) melted at higher temperatures (>1000 °C), spread on the surface, and combined with SiO_2, preventing further oxidation of the samples. This phenomenon correlated with the high weight retention of Si(B)CN/CF1200 and Si(B)CN/CF1500 samples, although the sample shapes deformed at higher temperatures. For the Si(Hf)CN/CF samples, the formation of HfO_2 and $Si_xO_yHf_z$ during heating contributed to the oxidation resistance of the samples. The $Si_xO_yHf_z$ liquid phase at higher temperatures limited the diffusion of oxygen, and the formation of HfO_2 acted as a grip to hold $Si_xO_yHf_z$ in place preventing further oxidation.[52]

The use of liquid-phase precursors to fabricate CMCs has reduced the cost of the composites and allows machining of the components in near-net-shape which eliminates the need of final machining. The current areas of the PDC CMCs are focused on the spatial and structural design of the CMCs as well as functional properties and applications such as load bearing structures,[53] brake components,[54] and aerothermal structural materials (thermal protection systems, combustion

Table 4. Comparison of Elemental Compositions of Oxidized Samples Determined by XPS

sample	Si (at. %)	C (at. %)	N (at. %)	O (at. %)	B (at. %)	Hf (at. %)
SiCN/CF800	30.88	15.87	0.26	52.99	NA	NA
SiCN/CF1000	26.07	9.03	0.31	64.59	NA	NA
SiCN/CF1200	30.85	11.89	0.27	56.98	NA	NA
SiCN/CF1500	29.58	12.93	0.27	57.21	NA	NA
Si(B)CN/CF800	20.78	15.12	0.78	51.64	11.69	NA
Si(B)CN/CF1000	21.62	14.79	0.44	50.43	12.72	NA
Si(B)CN/CF1200	25.01	8.28	0.7	53.05	12.97	NA
Si(B)CN/CF1500	26.73	2.06	0.16	60.4	10.65	NA
Si(Hf)CN/CF800	22.74	19.7	1.61	51.15	NA	4.8
Si(Hf)CN/CF1000	23.87	15.82	1.41	55.01	NA	3.89
Si(Hf)CN/CF1200	20.22	22.43	1.72	48.22	NA	7.4
Si(Hf)CN/CF1500	24.03	10.67	1.84	56.62	NA	6.84

https://doi.org/10.1021/acsomega.2c05916
ACS Omega 2022, 7, 45325−45335

chamber, and nozzle extensions).[55] However, there are some limitations of the current technologies that are used to fabricate CMCs. For example, the silicon-melt infiltration process produces residual silicon in CMCs that limits the operating temperature. The PIP technique has the possibility of shrinkage upon polymer-to-ceramic conversion, which degrades the strength of the CMCs, and multiple infiltration costs several days to cure. The chemical vapor infiltration technique creates porosity inside the CMCs, sometimes more than 10%, that causes poor mechanical and oxidation behavior. The goal of this work was to implement single-cycle infiltration to make enhanced CMCs with Si(B)CN and Si(Hf)CN ceramics and test their mechanical and oxidation behavior to show their potential for next-generation composites.

4. CONCLUSIONS

This study presented a scalable method to fabricate ceramic composites from single-source boron- and hafnium-modified PSZ precursors. Electron microscopy of the Si(B)CN/CF and Si(Hf)CN/CF samples confirmed the formation of ceramic matrix on the CF reinforcements. Raman, FTIR, and XPS characterization techniques outlined the polymer to ceramic conversion stages. Of the CMC minicomposites, the Si(Hf)-CN/CF sample showed the highest mechanical strength of ∼790 MPa and elastic modulus of 66.88 GPa. Efficiency of the oxidation resistance was also evident in all the SiCN/CF, Si(B)CN/CF, and Si(Hf)CN/CF CMC samples in spite of the complex architecture of the fiber and matrix damage. However, Si(Hf)CN/CF showed oxidation resistance up to 1500 °C due to the formation of $Si_xO_yHf_z$ liquid phase at higher temperatures (>1000 °C) with HfO_2.

■ ASSOCIATED CONTENT

Supporting Information

The Supporting Information is available free of charge at https://pubs.acs.org/doi/10.1021/acsomega.2c05916.

Data for optimization of preceramic polymer coatings on CF, Raman analysis spectra, additional data on tensile tests, post-tensile SEM images, and TGA analysis (PDF)

■ AUTHOR INFORMATION

Corresponding Author

Shakir Bin Mujib − *Department of Mechanical and Nuclear Engineering, Kansas State University, Manhattan, Kansas 66506, United States;* orcid.org/0000-0002-6699-420X; Email: sbmujib@ksu.edu

Authors

Mohammed Rasheed − *Department of Mechanical and Nuclear Engineering, Kansas State University, Manhattan, Kansas 66506, United States*

Gurpreet Singh − *Department of Mechanical and Nuclear Engineering, Kansas State University, Manhattan, Kansas 66506, United States*

Complete contact information is available at: https://pubs.acs.org/10.1021/acsomega.2c05916

Notes

The authors declare no competing financial interest.

■ ACKNOWLEDGMENTS

This manuscript has been authored by Honeywell Federal Manufacturing & Technologies LLC under Contract no. DE-NA-0002839 with the U.S. Department of Energy/National Nuclear Security Administration. The United States Government retains and the publisher, by accepting the article for publication, acknowledges that the United States Government retains a nonexclusive, paid-up, irrevocable, world-wide license to publish or reproduce the published form of this manuscript, or allow others to do so, for United States Government purposes. Singh is supported by the National Science Foundation (NSF) Partnerships for International Research and Education (PIRE) grant number 1743701. SEM and XPS were performed at the Nebraska Nanoscale Facility: National Nanotechnology Coordinated Infrastructure and the Nebraska Center for Materials and Nanoscience, supported by the NSF grant NNCI-1542182, and the Nebraska Research Initiative (NRI).

■ REFERENCES

(1) (a) Zhao, J. C.; Westbrook, J. H. Ultrahigh-Temperature Materials for Jet Engines. *MRS Bull.* **2003**, *28*, 622−630. (b) Padture, N. P. Advanced structural ceramics in aerospace propulsion. *Nat. Mater.* **2016**, *15*, 804−809. (c) Wang, Y.; Wu, H. Microstructure of friction surface developed on carbon fibre reinforced carbon-silicon carbide (Cf/C-SiC). *J. Eur. Ceram. Soc.* **2012**, *32*, 3509−3519.

(2) (a) Paul, A.; Jayaseelan, D. D.; Venugopal, S.; Zapata-Solvas, E.; Binner, J.; Vaidhyanathan, V.; Heaton, A.; Brown, P. M.; Lee, W. *UHTC Composites for Hypersonic Applications*; Wiley, 2012. (b) Baldus, P.; Jansen, M.; Sporn, D. Ceramic Fibers for Matrix Composites in High-Temperature Engine Applications. *Science* **1999**, *285*, 699−703. (c) Naslain, R.; Christin, F. SiC-Matrix Composite Materials for Advanced Jet Engines. *MRS Bull.* **2003**, *28*, 654−658.

(3) Zhang, H.; Liang, X.; Hu, Y.; Zhang, P.; Yang, L.; He, D.; Hua, M.; Tong, Y. Correlation of C/C preform density and microstructure and mechanical properties of C/C-ZrC-based ultra-high-temperature ceramic matrix composites. *Adv. Compos. Hybrid Mater.* **2021**, *4*, 743−750.

(4) Tong, Y.; Ren, Z.; Hu, Y.; Zhang, P.; Liang, X.; Chen, Y.; Yang, L.; Hua, M. Damage behavior and mechanism of C/C-SiC composite ablated under different environments. *Adv. Compos. Hybrid Mater.* **2022**, *5*, 1433−1438.

(5) Schomer, L.; Kütemeyer, M.; Liewald, M. Interface reactions occurring in metal-ceramic interpenetrating phase composites manufactured by using semi-solid forming technology. *Adv. Compos. Hybrid Mater.* **2020**, *3*, 222−230.

(6) Wen, Q.; Yu, Z.; Riedel, R. The fate and role of in situ formed carbon in polymer-derived ceramics. *Prog. Mater. Sci.* **2020**, *109*, 100623.

(7) (a) Friess, M.; Bill, J.; Golczewski, J.; Zimmermann, A.; Aldinger, F.; Riedel, R.; Raj, R. Crystallization of Polymer-Derived Silicon Carbonitride at 1873 K under Nitrogen Overpressure. *J. Am. Ceram. Soc.* **2002**, *85*, 2587−2589. (b) Bernardo, E.; Ponsot, I.; Colombo, P.; Grasso, S.; Porwal, H.; Reece, M. J. Polymer-derived SiC ceramics from polycarbosilane/boron mixtures densified by SPS. *Ceram. Int.* **2014**, *40*, 14493−14500. (c) Kleebe, H.-J.; Gregori, G.; Babonneau, F.; Blum, Y. D.; MacQueen, D. B.; Masse, S. Evolution of C-rich SiOC ceramics: Part I. Characterization by integral spectroscopic techniques: Solid-state NMR and Raman spectroscopy. *Int. J. Mater. Res.* **2006**, *97*, 699−709.

(8) Colombo, P.; Mera, G.; Riedel, R.; Soraru, G. D. Polymer-derived ceramics: 40 years of research and innovation in advanced ceramics. *J. Am. Ceram. Soc.* **2010**, *93*, 1805−1837.

(9) Zimmermann, A.; Bauer, A.; Christ, M.; Cai, Y.; Aldinger, F. High-temperature deformation of amorphous Si−C−N and Si−B−C−N ceramics derived from polymers. *Acta Mater.* **2002**, *50*, 1187−1196.

(10) Harshe, R.; Balan, C.; Riedel, R. Amorphous Si(Al)OC ceramic from polysiloxanes: bulk ceramic processing, crystallization behavior and applications. *J. Eur. Ceram. Soc.* **2004**, *24*, 3471−3482.
(11) Anand, R.; Nayak, B. B.; Behera, S. K. Coarsening kinetics of nanostructured ZrO2 in Zr-doped SiCN ceramic hybrids. *J. Alloys Compd.* **2019**, *811*, 151939.
(12) Tang, X.; Yu, Y.; Yang, D. SiO2/TiO2 fibers from titanium-modified polycarbosilane. *J. Mater. Sci.* **2010**, *45*, 2670−2674.
(13) Sun, J.; Wen, Q.-B.; Li, T.; Wiehl, L.; Fasel, C.; Feng, Y.; De Carolis, D.; Yu, Z.-J.; Fu, Q.-G.; Riedel, R. Phase evolution of SiOC-based ceramic nanocomposites derived from a polymethylsiloxane modified by Hf- and Ti-alkoxides. *J. Am. Ceram. Soc.* **2020**, *103*, 1436−1445.
(14) Ren, Z.; Mujib, S. B.; Singh, G. High-Temperature Properties and Applications of Si-Based Polymer-Derived Ceramics: A Review. *Materials* **2021**, *14*, 614.
(15) Tong, Y.; Zhu, W.; Bai, S.; Hu, Y.; Xie, X.; Li, Y. Thermal shock resistance of continuous carbon fiber reinforced ZrC based ultra-high temperature ceramic composites prepared via Zr-Si alloyed melt infiltration. *Mater. Sci. Eng., A* **2018**, *735*, 166−172.
(16) Mileiko, S. T. 4.09-Constituent Compatibility and Microstructural Stability. In *Comprehensive Composite Materials*; Kelly, A., Zweben, C., Eds.; Pergamon, 2000; pp 265−287.
(17) (a) Johannisson, W.; Ihrner, N.; Zenkert, D.; Johansson, M.; Carlstedt, D.; Asp, L. E.; Sieland, F. Multifunctional performance of a carbon fiber UD lamina electrode for structural batteries. *Compos. Sci. Technol.* **2018**, *168*, 81−87. (b) Xu, J.; Lindbergh, G.; Varna, J. Carbon fiber composites with battery function: Stresses and dimensional changes due to Li-ion diffusion. *J. Compos. Mater.* **2018**, *52*, 2729−2742. (c) Dang, C.; Mu, Q.; Xie, X.; Sun, X.; Yang, X.; Zhang, Y.; Maganti, S.; Huang, M.; Jiang, Q.; Seok, I.; et al. Recent progress in cathode catalyst for nonaqueous lithium oxygen batteries: a review. *Adv. Compos. Hybrid Mater.* **2022**, *5*, 606−626.
(18) He, Y.; Zhou, M.; Mahmoud, M. H. H.; Lu, X.; He, G.; Zhang, L.; Huang, M.; Elnaggar, A. Y.; Lei, Q.; Liu, H.; et al. Multifunctional wearable strain/pressure sensor based on conductive carbon nanotubes/silk nonwoven fabric with high durability and low detection limit. *Adv. Compos. Hybrid Mater.* **2022**, *5*, 1939−1950.
(19) Yuan, B.; Wang, Y.; Elnaggar, A. Y.; Azab, I. H. E.; Huang, M.; Mahmoud, M. H. H.; El-Bahy, S. M.; Guo, M. Physical vapor deposition of graphitic carbon nitride (g-C3N4) films on biomass substrate: optoelectronic performance evaluation and life cycle assessment. *Adv. Compos. Hybrid Mater.* **2022**, *5*, 813−822.
(20) Gao, S.; Zhao, X.; Fu, Q.; Zhang, T.; Zhu, J.; Hou, F.; Ni, J.; Zhu, C.; Li, T.; Wang, Y.; et al. Highly transmitted silver nanowires-SWCNTs conductive flexible film by nested density structure and aluminum-doped zinc oxide capping layer for flexible amorphous silicon solar cells. *J. Mater. Sci. Technol.* **2022**, *126*, 152−160.
(21) Riedel, R.; Kienzle, A.; Dressler, W.; Ruwisch, L.; Bill, J.; Aldinger, F. A silicoboron carbonitride ceramic stable to 2,000 °C. *Nature* **1996**, *382*, 796−798.
(22) Saha, A.; Raj, R.; Williamson, D.; Kleebe, H.-J. Characterization of nanodomains in polymer-derived SiCN ceramics employing multiple techniques. *J. Am. Ceram. Soc.* **2005**, *88*, 232−234.
(23) Singh, G.; Bhandavat, R. Boron-modified silazanes for synthesis of SiBNC ceramics. U.S. Patent 20,150,030,856 A1, 2016.
(24) (a) Singh, G.; David, L. Aluminum-modified polysilazanes for polymer-derived ceramic nanocomposites. U.S. Patent 20,160,009,741 A1, 2018. (b) Singh, G.; David, L. Silicon-based polymer-derived ceramic composites comprising H-BN nanosheets. U.S. Patent 20,170,144,935 A1, 2018.
(25) Lee, S. H.; Weinmann, M.; Aldinger, F. Processing and properties of C/Si−B−C−N fiber−reinforced ceramic matrix composites prepared by precursor impregnation and pyrolysis. *Acta Mater.* **2008**, *56*, 1529−1538.
(26) Weinmann, M.; Schuhmacher, J.; Kummer, H.; Prinz, S.; Peng, J.; Seifert, H. J.; Christ, M.; Müller, K.; Bill, J.; Aldinger, F. Synthesis and Thermal Behavior of Novel Si−B−C−N Ceramic Precursors. *Chem. Mater.* **2000**, *12*, 623−632.
(27) Kong, J.; Wang, M.; Zou, J.; An, L. Soluble and Meltable Hyperbranched Polyborosilazanes toward High-Temperature Stable SiBCN Ceramics. *ACS Appl. Mater. Interfaces* **2015**, *7*, 6733−6744.
(28) Zhao, H.; Chen, L.; Luan, X.; Zhang, X.; Yun, J.; Xu, T. Synthesis, pyrolysis of a novel liquid SiBCN ceramic precursor and its application in ceramic matrix composites. *J. Eur. Ceram. Soc.* **2017**, *37*, 1321−1329.
(29) Ionescu, E.; Papendorf, B.; Kleebe, H.-J.; Riedel, R. Polymer-Derived Silicon Oxycarbide/Hafnia Ceramic Nanocomposites. Part II: Stability Toward Decomposition and Microstructure Evolution at T ≫1000 °C. *J. Am. Ceram. Soc.* **2010**, *93*, 1783−1789.
(30) Wen, Q.; Luan, X.; Wang, L.; Xu, X.; Ionescu, E.; Riedel, R. Laser ablation behavior of SiHfC-based ceramics prepared from a single-source precursor: Effects of Hf-incorporation into SiC. *J. Eur. Ceram. Soc.* **2019**, *39*, 2018−2027.
(31) Yuan, J.; Hapis, S.; Breitzke, H.; Xu, Y.; Fasel, C.; Kleebe, H.-J.; Buntkowsky, G.; Riedel, R.; Ionescu, E. Single-Source-Precursor Synthesis of Hafnium-Containing Ultrahigh-Temperature Ceramic Nanocomposites (UHTC-NCs). *Inorg. Chem.* **2014**, *53*, 10443−10455.
(32) Wei, Y.; Yang, Y.; Liu, M.; Li, Q.; Huang, Z. Oxidation mechanism and kinetics of SiBCN/HfC ceramic composites at high temperatures. *J. Mater. Res. Technol.* **2020**, *9*, 2289−2298.
(33) Miao, Y.; Zhang, F.; Yang, Z.; Jia, D.; Zhou, Y. Incorporation of BN-coated carbon fibers into ZrB2/SiBCN ceramic composites and their ablation behavior. *J. Eur. Ceram. Soc.* **2020**, *40*, 1078−1085.
(34) Dong, B.; Han, Y.; Wang, T.; Lei, Z.; Chen, Y.; Wang, F.; Abadikhah, H.; Khan, S. A.; Hao, L.; Xu, X.; et al. Hard SiOC Microbeads as a High-Performance Lithium-Ion Battery Anode. *ACS Appl. Energy Mater.* **2020**, *3*, 10183−10191.
(35) Mujib, S. B.; Ribot, F.; Gervais, C.; Singh, G. Self-supporting carbon-rich SiOC ceramic electrodes for lithium-ion batteries and aqueous supercapacitors. *RSC Adv.* **2021**, *11*, 35440−35454.
(36) Zhang, Q.; Yang, Z.; Jia, D.; Chen, Q.; Zhou, Y. Synthesis and structural evolution of dual-boron-source-modified polysilazane derived SiBCN ceramics. *New J. Chem.* **2016**, *40*, 7034−7042.
(37) (a) Kim, K.; Ju, H.; Kim, J. Pyrolysis behavior of polysilazane and polysilazane-coated-boron nitride for high thermal conductive composite. *Compos. Sci. Technol.* **2017**, *141*, 1−7. (b) Chavez, R.; Ionescu, E.; Balan, C.; Fasel, C.; Riedel, R. Effect of ambient atmosphere on crosslinking of polysilazanes. *J. Appl. Polym. Sci.* **2011**, *119*, 794−802.
(38) Song, C.; Liu, X.; Ye, F.; Liu, Y.; Cheng, L. Mechanical and dielectric properties of SiCf/BN/SiBCN composites via different synthesis technologies. *J. Eur. Ceram. Soc.* **2019**, *39*, 4417−4423.
(39) Galuska, A. A.; Uht, J. C.; Marquez, N. Reactive and nonreactive ion mixing of Ti films on carbon substrates. *J. Vac. Sci. Technol., A* **1988**, *6*, 110−122.
(40) Ma, S. L.; Xu, B.; Xu, K. W.; Wu, X. L.; Chu, P. K. Annealing behavior and hardness enhancement of amorphous SiCN thin films. *J. Vac. Sci. Technol., A* **2007**, *25*, 1407−1410.
(41) Gouin, X.; Grange, P.; Bois, L.; L'Haridon, P.; Laurent, Y. Characterization of the nitridation process of boric acid. *J. Alloys Compd.* **1995**, *224*, 22−28.
(42) Barreca, D.; Milanov, A.; Fischer, R. A.; Devi, A.; Tondello, E. Hafnium oxide thin film grown by ALD: An XPS study. *Surf. Sci. Spectra* **2007**, *14*, 34−40.
(43) Bhandavat, R.; Feldman, A.; Cromer, C.; Lehman, J.; Singh, G. Very High Laser-Damage Threshold of Polymer-derived Si(B)CN-Carbon Nanotube Composite Coatings. *ACS Appl. Mater. Interfaces* **2013**, *5*, 2354−2359.
(44) (a) Lee, S.; Yun, D.-J.; Rhee, S.-W.; Yong, K. Atomic layer deposition of hafnium silicate film for high mobility pentacene thin film transistor applications. *J. Mater. Chem.* **2009**, *19*, 6857−6864. (b) Mullapudi, G. S. R.; Velazquez-Nevarez, G. A.; Avila-Avendano, C.; Torres-Ochoa, J. A.; Quevedo-López, M. A.; Ramírez-Bon, R. Low-Temperature Deposition of Inorganic−Organic HfO2−PMMA Hybrid Gate Dielectric Layers for High-Mobility ZnO Thin-Film Transistors. *ACS Appl. Electron. Mater.* **2019**, *1*, 1003−1011.

https://doi.org/10.1021/acsomega.2c05916
ACS Omega 2022, 7, 45325−45335

(45) (a) Callaway, E. B.; Zok, F. W. Strengths of ceramic fiber bundles: Theory and practice. *J. Am. Ceram. Soc.* **2017**, *100*, 5306−5317. (b) Ikarashi, Y.; Ogasawara, T.; Okuizumi, S.-i.; Aoki, T.; Davies, I. J.; Lamon, J. Direct comparison between monofilament and multifilament tow testing for evaluating the tensile strength distribution of SiC fibers. *J. Eur. Ceram. Soc.* **2022**, *42*, 1928−1937.
(46) (a) Woodford, D. A.; Van Steele, D. R.; Brehm, J. A.; Timms, L. A.; Palko, J. E. Testing the tensile properties of ceramic-matrix composites. *JOM* **1993**, *45*, 57−63. (b) Pétursson, J. Performance characterization of ceramic matrix composites through uniaxial monotonic tensile testing, M.Sc Thesis, Embry-Riddle Aeronautical University, 2016
(47) (a) Azarnoush, S.; Laubscher, F.; Zoli, L.; Raj, R. Additive Manufacturing of SiCN Ceramic Matrix for SiC Fiber Composites by Flash Pyrolysis of Nanoscale Polymer Films. *J. Am. Ceram. Soc.* **2016**, *99*, 1855−1858. (b) Berbon, M.; Calabrese, M. Effect of 1600°C Heat Treatment on C/SiC Composites Fabricated by Polymer Infiltration and Pyrolysis with Allylhydridopolycarbosilane. *J. Am. Ceram. Soc.* **2002**, *85*, 1891−1893.
(48) Bansal, N. P.; Eldridge, J. I. *Effects of Fiber/Matrix Interface and Its Composition on Mechanical Properties of Hi-Nicalon/Celsian Composites*, 1999,
(49) Kumar, S.; Rai, S. B.; Rath, C. Multifunctional role of dysprosium in HfO2: stabilization of the high temperature cubic phase, and magnetic and photoluminescence properties. *Phys. Chem. Chem. Phys.* **2017**, *19*, 18957−18967.
(50) Raj, R.; An, L.; Shah, S.; Riedel, R.; Fasel, C.; Kleebe, H.-J. Oxidation Kinetics of an Amorphous Silicon Carbonitride Ceramic. *J. Am. Ceram. Soc.* **2001**, *84*, 1803−1810.
(51) Lu, B.; Zhang, Y. Oxidation behavior of SiC−SiBCN ceramics. *Ceram. Int.* **2015**, *41*, 1023−1030.
(52) Verdon, C.; Szwedek, O.; Allemand, A.; Jacques, S.; Le Petitcorps, Y.; David, P. High temperature oxidation of two- and three-dimensional hafnium carbide and silicon carbide coatings. *J. Eur. Ceram. Soc.* **2014**, *34*, 879−887.
(53) Krenkel, W. Carbon Fiber Reinforced CMC for High-Performance Structures. *Int. J. Appl. Ceram. Technol.* **2004**, *1*, 188−200.
(54) (a) Renz, R.; Seifert, G.; Krenkel, W. Integration of CMC Brake Disks in Automotive Brake Systems. *Int. J. Appl. Ceram. Technol.* **2012**, *9*, 712−724. (b) Fan, S.; Yang, C.; He, L.; Du, Y.; Krenkel, W.; Greil, P.; Travitzky, N. Progress of ceramic matrix composites brake materials for aircraft application. *Rev. Adv. Mater. Sci.* **2016**, *44*, 313−325.
(55) (a) Boehrk, H.; Weihs, H.; Elsäßer, H. Hot Structure Flight Data of a Faceted Atmospheric Reentry Thermal Protection System. *Int. J. Mech. Ind. Aero. Eng.* **2019**, *2019*, 1. (b) Schmidt, S.; Beyer, S.; Knabe, H.; Immich, H.; Meistring, R.; Gessler, A. Advanced ceramic matrix composite materials for current and future propulsion technology applications. *Acta Astronaut.* **2004**, *55*, 409−420. (c) Zhu, D. *Aerospace Ceramic Materials: Thermal, Environmental Barrier Coatings and SiC/SiC Ceramic Matrix Composites for Turbine Engine Applications*; National Aeronautics and Space Administration, 2018.

https://doi.org/10.1021/acsomega.2c05916
ACS Omega 2022, 7, 45325−45335